Bisaryloxime Ethers as Potent Inhibitors of Transthyretin Amyloid Fibril Formation

Steven M. Johnson,[†] H. Michael Petrassi,[†] Satheesh K. Palaninathan,[‡] Nilofar N. Mohamedmohaideen,[‡] Hans E. Purkey,[†] Christopher Nichols,[†] Kyle P. Chiang,[†] Traci Walkup,[†] James C. Sacchettini,[‡] K. Barry Sharpless,[†] and Jeffery W. Kelly*[,†]

Department of Chemistry and the Skaggs Institute for Chemical Biology, The Scripps Research Institute, 10550 N. Torrey Pines Rd., La Jolla, Califonia 92037, and Department of Biochemistry and Biophysics, Texas A&M University, College Station, Texas 77843-2128

Received September 3, 2004

Amyloid fibril formation by the plasma protein transthyretin (TTR), requiring rate-limiting tetramer dissociation and monomer misfolding, is implicated in several human diseases. Amyloidogenesis can be inhibited through native state stabilization, mediated by small molecule binding to TTR's primarily unoccupied thyroid hormone binding sites. New native state stabilizers have been discovered herein by the facile condensation of arylaldehydes with aryloxyamines affording a bisarylaldoxime ether library. Of the library's 95 compounds, 31 were active inhibitors of TTR amyloid formation in vitro. The bisaryloxime ethers selectively stabilize the native tetrameric state of TTR over the dissociative transition state under amyloidogenic conditions, leading to an increase in the dissociation activation barrier. Several bisaryloxime ethers bind selectively to TTR in human blood plasma over the plethora of other plasma proteins, a necessary attribute for efficacy in vivo. While bisarylaldoxime ethers are susceptible to degradation by N−O bond cleavage, this process is slowed by their binding to TTR. Furthermore, the degradation rate of many of the bisarylaldoxime ethers is slow relative to the half-life of plasma TTR. The bisaryloxime ether library provides valuable structure−activity relationship insight for the development of structurally analogous inhibitors with superior stability profiles, should that prove necessary.

Introduction

The process of transthyretin (TTR) amyloidogenesis leads to peripheral neuropathy, organ dysfunction, and, in rare cases, central nervous system pathology.[1−7] The disease caused by wild type (WT) TTR deposition, senile systemic amyloidosis (SSA), is a late-onset cardiomyopathy affecting 10−25% of the population over age 80.[5] The remaining TTR-based amyloid diseases associated with point mutations are grouped into two broad classifications: familial amyloid cardiomyopathy (FAC)[6] and familial amyloid polynueropathy (FAP).[7] There are over 100 TTR mutations that cause the familial amyloidoses, the exact age of onset, tissue selectivity, and severity of which are dependent on the energetics of the specific mutation, the individual's genetic background, and possibly environmental factors.[8,9]

The only treatment currently available for FAP is gene therapy mediated by surgical replacement of the patient's liver, the organ secreting TTR subject to misfolding into the blood stream.[10] The disadvantages of this approach include its invasiveness for both the donor and recipient, the requirement for life-long immune suppression, and the limited effectiveness for some mutations for reasons that are not yet clear.[11] Currently there is no effective treatment for SSA associated with WT-TTR deposition. Therefore, a generally applicable, small molecule therapeutic strategy for all TTR-based amyloid diseases would be welcomed.

Interallelic *trans*-suppression in a compound heterozygous family enabled by the inclusion of T119M transthyretin subunits into tetramers otherwise composed of disease associated subunits (V30M) demonstrates that kinetic stabilization of TTR is sufficient to ameliorate FAP.[12−14] The efficacy of *trans*-suppression implies that small molecule native state kinetic stabilization should also ameliorate amyloidosis.[15,16] The utility of small molecules to tune the free energy landscape of proteins to prevent misfolding associated with disease has now been demonstrated in several instances.[12,15−20]

TTR is a 127-residue β-sheet-rich homotetramer characterized by 222 molecular symmetry, possessing two thyroxine (T_4) binding sites.[21,22] The vast majority (>99%) of the TTR T_4 binding capacity in both the cerebrospinal fluid (CSF) and blood plasma is unutilized because of the high concentration of TTR and the presence of thyroid binding globulin (blood) and albumin (blood and CSF), which are also carriers of T_4.[23−25] Rate-limiting tetramer dissociation is required for amyloidogenesis[26−29] but is not sufficient,[30] as the resulting folded monomer must also undergo partial denaturation to misassemble.[26,28−31] Previous studies demonstrate that T_4 binding inhibits TTR aggregation by kinetic stabilization of the native state. The activation barrier for dissociation is increased by preferential stabilization of

* To whom correspondence should be addressed: Phone: (858) 784-9605, Fax: (858) 784-9610, email: jkelly@scripps.edu.
[†] The Scripps Research Institute.
[‡] Texas A&M University.

10.1021/jm049274d CCC: $30.25
Published on Web 02/08/2005

Scheme 1. General Approach for the Formation of the Bisaryloxime Ether (X = O) and Bisarylhydrazone (X = NH) Libraries

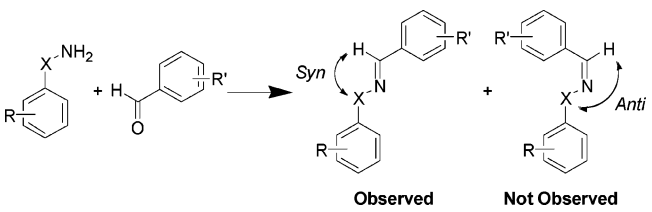

the native tetramer relative to the dissociative transition state.[12,32,33]

Screening, structure-based design, and lead compound optimization by parallel synthesis has led to several other structurally distinct classes of potent TTR amyloidogenesis inhibitors.[12,15,16,20,32−44] Effective inhibitors generally have two aryls linked directly or through a spacer such as an amine, an ether, or an ethylene bridge. Optimally, one aryl is functionalized with halogens or aliphatic groups (typically occupying the inner cavity of the thyroxine binding site) and the other by a hydroxyl and/or carboxylic acid (which can interact electrostatically with the Lys15 ϵ-NH_3^+ and/or Glu54 carboxyl groups at the periphery of the outer binding cavity).[12,15,16,20,32−44] Both cavities have hydrophobic depressions called halogen binding pockets, that are complemented by the aryl substructures and their hydrophobic substituents.

After considering the orientation and placement of substituted aromatics in numerous TTR•(inhibitor)$_2$ cocrystal structures, synthetic accessibility, and the potential for future high-throughput dynamic combinatorial library analyses,[45,46] we chose to explore the aldoxime ether moiety to link the two aryl rings. There are several FDA approved antibacterial agents containing the oxime ether moiety, suggesting that this substructure is compatible with human biology.[47] The goal of this study is to find bisarylaldoxime ether structures that bind with high affinity to TTR in human blood plasma[48] and stabilize the native state against amyloidogenesis.[12,16]

Results and Discussion

Design of the Oxime Ether Library. Aryloxyamines are required as starting materials to couple with arylaldehydes to generate the desired bisaryloxime ether library (Scheme 1, X = O). This reaction could potentially produce two stereoisomers about the imine linkage (denoted *syn* and *anti*, i.e., the aldehyde proton could be oriented *cis* or *trans*, respectively, to the phenoxy oxygen represented by X, Scheme 1); however, only the *syn*-isomer was expected (and observed, see below) based on literature precedent.[49−55]

The oxime ether substituents and substitution patterns were chosen on the basis of structural features identified in other potent TTR amyloidogenesis inhibitors (Figure 1).[12,15,16,20,32−44] The aryloxyamines chosen (**1**−**8**) had the same substitution patterns as the arylaldehydes, except for the absence of *p*-CF_3 (**i**) and the thyroxine-like substitution patterns (**e** and **f**) in the aryloxyamines. Unfortunately, the only commercially available aryloxyamine is phenoxyamine; thus, we and others have developed methodology for the synthesis of the aryloxyamine building blocks required to prepare

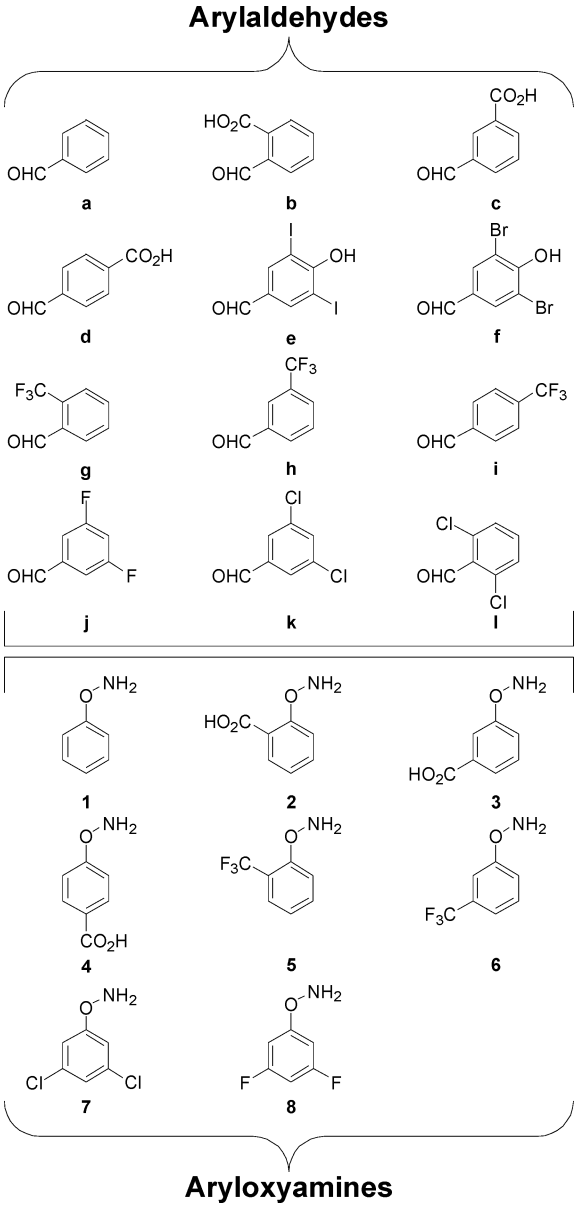

Figure 1. Structures of aryloxyamine (**1**−**8**) and benzaldehyde (**a**−**l**) components used to synthesize the bisaryloxime ether library (see Scheme 1).

the bisaryloxime ether library.[56−59] In contrast, over 150 arylhydrazines are commercially available for coupling to readily available arylaldehydes to produce a bisarylhydrazone library (Scheme 1, X = NH). Because analogous bisaryloxime ethers and bisarylhydrazones (hereafter referred to as oxime ethers and hydrazones, respectively) were assumed to be isostructural with one another, the rapid automated synthesis of a hydrazone library (Figure S1) was performed to query whether this structural class of inhibitors would likely be active (Table S1).

Characterization and Crystallographic Comparison of Oxime Ethers and Hydrazones. To confirm their presumed isostructural nature, pairs of analogous oxime ethers and hydrazones based on scaffolds **5b/d** (Figure 1) and **26b/d** (Figure S1), respectively, were synthesized and crystallized, and their structures were determined by X-ray diffraction. Comparison of the oxime ether and hydrazone structures by crystallography reveals that the analogous compounds

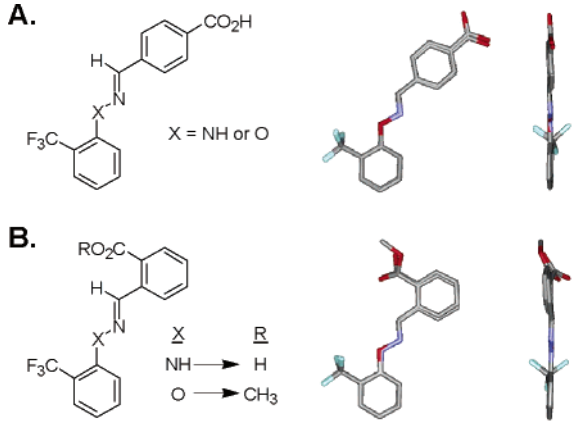

Figure 2. Overlays of analogous bisarylhydrazone and bisaryloxime ether structures derived from X-ray crystallographic data: (A) Superposition of bisaryloxime ether **5d** and its analogous bisarylhydrazone (**26d**, Figure S1). (B) Superposition of bisaryloxime ether **5b** methyl ester and its analogous bisarylhydrazone carboxylic acid (**26b**, Figure S1).

are nearly superimposable on one another (Figure 2). All four crystal structures display *syn*-imine linkages, further supporting the predominance of this isomer.[49−55]

HPLC and LC−MS traces of all the crude reaction mixtures associated with hydrazone (>94% purity) and oxime ether (>95% purity) library production showed primarily one peak, suggesting the predominance of a single isomer (*syn*-imine linkage inferred from precedent and supported by X-ray crystallography). In principle, it is possible that both the *syn*- and the *anti*-isomers coelute or rapidly interconvert and crystallize preferentially as the *syn*-isomer; however, the ^{1}H and ^{13}C NMR spectra of the hydrazones and oxime ethers synthesized by traditional means exhibit resonances consistent with a single isomer (literature precedence demonstrates that the preferred *syn*-isomer is distinguishable from the *trans*-isomer by NMR at room temperature).[49−54]

Synthesis and Activity of Oxime Ether Library. We were confident that if the hydrazones (all >94% purity) displayed inhibitory activity, the equivalent oxime ether library would also produce TTR amyloidogenesis inhibitors. Several of the bisarylhydrazones displayed potent inhibition of TTR amyloidogenesis (Table S1), justifying the preparation and evaluation of an analogous oxime ether library. Aqueous hydrazone instability (owing primarily to Schiff base hydrolysis) and the biological toxicity of hydrazones provide further incentive to prepare the bisaryloxime ether library. Two synthetic strategies were employed for the preparation of the aryloxyamines required to make the bisaryloxime ether library. In the first, a copper-mediated cross-coupling of *N*-hydroxyphthalimide (NHP) with arylboronic acids affords the desired aryloxyamines after hydrazinolysis (Scheme 2A).[57] Aryloxyamines isolated as either free bases (**3**, **6**, and **7**) or precipitated as their hydrochloride salts (**1** and **8**) were synthesized in good to moderate overall yields using this methodology.

The copper-mediated coupling methodology appears to be intolerant of *o*-halide or *o*-CF_3 substituents on the arylboronic acid.[57] Furthermore, hydrazinolysis, required for the deprotection of the *N*-hydroxyphthalimide intermediates, does not succeed for aryloxyamines bearing *o*-carboxyl substituents. After exploring several

Scheme 2. Synthesis of Substituted Phenoxyamines: (A) Copper-Mediated Cross Coupling of *N*-Hydroxyphthalimide with Arylboronic Acids and (B) Nucleophilic Aromatic Substitution of Electron Deficient Flourobenzenes by Ethyl *N*-Hydroxyacetimidate[a]

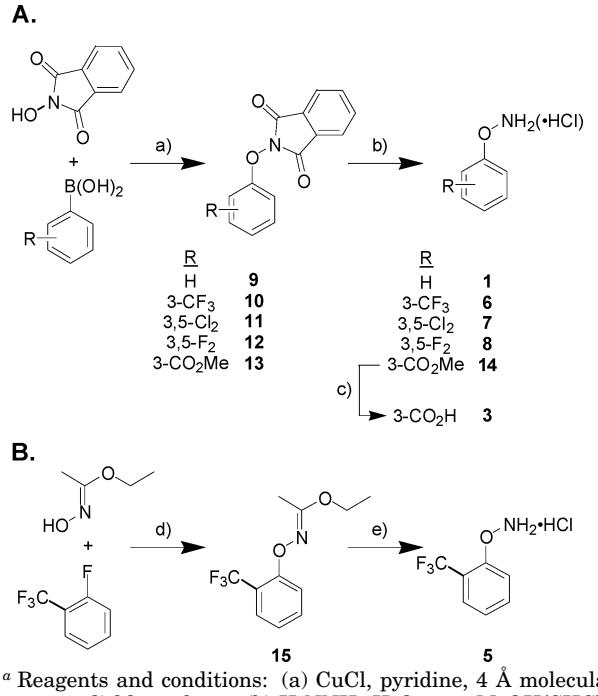

[a] Reagents and conditions: (a) CuCl, pyridine, 4 Å molecular sieves, 1,2-dichloroethane; (b) $H_2NNH_2 \cdot H_2O$, 10% MeOH/$CHCl_3$; (c) $LiOH \cdot H_2O$, THF/MeOH/H_2O; (d) ^{t}BuOK, DMF, 80°C; (e) $HClO_4$, 1,4-dioxane.

other methods, the nucleophilic aromatic substitution of electron-deficient flourobenzenes by ethyl *N*-hydroxyacetimidate was selected to complement the first method (Scheme 2B).[58] Nucleophilic attack of ethyl *N*-hydroxyacetimidate on 2-trifluoromethylflourobenzene gave an excellent yield of **15** (89%), which upon acidic hydrolysis gave aryloxyamine **5** (96% yield), utilized as its HCl salt. A variation on this methodology was used to prepare oxime ethers derived from the equivalents of **2** and **4** (see below).

Aryloxyamines **1** and **5**−**8** were used to generate a portion of the oxime ether library (Figure 1). Reactions between arylaldehydes (0.1 M) and aryloxyamines (0.125 M) in the presence of acetic acid (0.08 M) in DMSO afforded the oxime ethers in near quantitative yields within 24 h at 25 °C (all the phenoxyamines and hydrazines were tested as TTR amyloid inhibitors, owing to their use in excess in the library syntheses, revealing no inhibition). Five aryloxyamines (**1** and **5**−**8**) and 12 aldehydes (**a**−**l**) were condensed in all possible combinations to yield 60 oxime ethers using a Gilson 215 liquid handler in a single compound per well format. Reactions were analyzed by LC−MS to determine yield (98−100%, based on aldehyde consumption, see Experimental Section) and product purity (>95%) in all wells, with all products displaying their expected masses. In the seven cases (**1e**, **5d**−**f**, **7e**, and **8e**−**f**) where pure compounds were synthesized conventionally and complete characterization performed (see Supporting Information experimental), HPLC coelution confirmed product structures and purity.

The remaining members of the oxime ether library were prepared by traditional synthetic procedures and

Scheme 3. Synthesis of Bisaryloxime Ethers by a *trans*-Imination Approach[a]

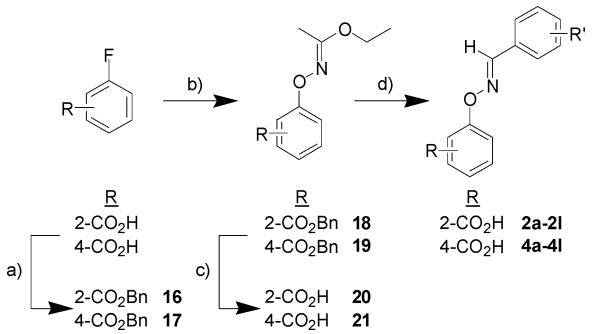

[a] Reagents and conditions: (a) benzyl alcohol, DCC, cat. DMAP, CH_2Cl_2; (b) ethyl *N*-hydroxyacetimidate, ^{t}BuOK, DMF; (c) LiOH·H_2O, THF/MeOH/H_2O; (d) R′-benzaldehyde (**a**−**l**), 70% $HClO_4$, 1,4-dioxane.

isolated in milligram quantities (see Experimental Section and Supporting Information for complete characterization data and Table S2 for compound purity as determined by RP-HPLC). *O*-(3-Carboxyphenyl)hydroxylamine (**3**) was condensed with arylaldehydes **a**−**l** in the presence of catalytic HCl to afford oxime ethers **3a**−**l** in moderate to excellent yields. Compounds **20** and **21** were prepared in 45 and 51% overall yields, respectively, using the ethyl *N*-hydroxyacetimidate S_NAr procedures (Scheme 3). The arylacetimidates were not hydrolyzed to the corresponding aryloxyamines **2** and **4**, instead they were mixed with stoichiometric amounts of arylaldehydes under acidic conditions to afford oxime ethers **2a**−**l** and **4a**−**l** directly in moderate to excellent yields (oxime ether **2b** was not isolable due to instability).

The inhibitory activity of the oxime ethers (7.2 μM) against acid-mediated (pH 4.4) TTR (3.6 μM) amyloid formation is summarized in Table 1. Of the 95 oxime ethers synthesized, 31 show good efficacy, reducing TTR amyloid formation to <10% of that exhibited by WT-TTR in the absence of inhibitor (90% inhibition, blue), nine exhibit moderate activity (11−30% fibril formation, green), and the remaining 55 display poor activity (yellow).

Oxime ethers derived from benzaldehydes with a thyroxine-like substitution pattern (Table 1, rows e and f) are highly efficacious (all 16 displayed >90% inhibition), even when coupled with an unsubstituted phenoxyamine, a coupling that typically results in poor oxime ether inhibitors. These results challenge previous beliefs that appropriate substituents are required on both rings to achieve inhibition.

Additional oxime ethers resulting from the condensation of halogenated aryloxyamines with *m*- or *p*-carboxybenzaldehydes or vice versa produced potent inhibitors, irrespective of which ring bears the carboxylic acid substituent. These results suggest that binding orientations may change to preserve electrostatic interactions with the ϵ-NH_3^+ group of Lys15. No oxime ethers derived from *o*-carboxybenzaldehyde produce good inhibitors. The activity of the carboxybenzaldehyde derived oxime ethers ranked from best to worst is *meta* > *para* > *ortho*, similar to that of oxime ethers derived from the carboxyphenoxyamines: *meta* ≈ *para* > *ortho*. Oxime ethers bearing carboxylic acids or halogens on both rings (excluding T_4-like substitution) displayed moderate activity at best.

Although the facility with which arylaldehydes and phenoxyamines condense lends itself to a dynamic combinatorial library approach,[45,46] a potential complication that lowered the priority of these experiments is our previous report that inhibition is typically maximal with two different small molecules bound owing to the allosteric communication between the two binding sites.[37] Hence, the structure−activity relationship data may be complicated by the influence of combinations of inhibitors produced in a dynamic combinatorial library.

Bisarylaldoxime Ether Stability. Although many bisarylaldoxime ethers are potent inhibitors of TTR amyloidogenesis (Table 1), they exhibit a range of stabilities in either acidic or basic aqueous media (first-order degradation half-lives range from hours to days in the absence of TTR). While the oxime ethers, unlike the hydrazones, appear stable toward Schiff base hydrolysis in neutral and basic conditions, they can still slowly decompose with first-order kinetics apparently by cleavage of their N−O bond to afford a phenol and an arylnitrile. This N−O bond cleavage, while precedented at higher temperatures, was not expected under such mild conditions.[60−67]

The oxime ethers are qualitatively more stable than the analogous hydrazones according to their apparent degradation "half-lives" (apparent hydrazone "half-lives" refer to the time required for 50% disappearance, as the degradation process is not first-order). Electron-donating groups and *ortho*-substituents on either aromatic ring appear to increase the degradation rate of both the bisarylaldoxime ethers and bisarylhydrazones. A detailed analysis of the stability of bisarylhydrazones and bisaryloxime ethers is in progress and will be reported elsewhere. However, those compounds displaying inherent instability may still be useful as pharmacological tools. We will also soon evaluate the activity and stability of amine analogues produced by reduction of the imine.

In general, inhibitor (7.2 μM) binding to TTR (3.6 μM) acts to stabilize the compounds from degradation under acid-mediated fibril formation conditions (pH 4.4, 37 °C, 72 h). For 11 of the best inhibitors (<10% fibril formation), RP-HPLC analysis reveals that >74% of the initial oxime ether remains at the end of the acid-mediated fibril formation assay (Table 2). The least stable inhibitors (**1e**, **1f**, **2k**, **3g**, **5d***) undergo nearly complete degradation in the absence of TTR within 72 h; however, its presence maintains >74% of the initial dose. Notably, inhibitor **5e** exhibits no decomposition in the presence of TTR. This helps explain why many of the labile bisaryloxime inhibitors prove to be excellent inhibitors of TTR amyloidogenesis: not only do the inhibitors bind to TTR's thyroid hormone binding sites and impose kinetic stabilization on the TTR tetramer[12] but TTR binding also stabilizes the inhibitors against degradation.

Analyses were also performed to help confirm that the activities were primarily due to individual oxime ethers and not their proposed degradation products. To determine whether the degradative byproducts contribute to the observed inhibitor efficacy, the corresponding phenols and nitriles (in the case of the oxime ethers), anilines (in the case of the hydrazones), and aldehydes (both oxime ethers and hydrazones) were analyzed for

Table 1. Oxime Ether Activity (7.2 μM) against WT-TTR (3.6 μM) Amyloid Fibril Formation at pH 4.4 (72 h)[a]

Arylaldehyde Component	Aryloxyamine Component: H (1)	2-CO_2H (2)	3-CO_2H (3)	4-CO_2H (4)	2-CF_3 (5)	3-CF_3 (6)	3,5-Cl_2 (7)	3,5-F_2 (8)
H (a)	96	91	50	32	56	83	39	87
2-CO_2H (b)	91	Unstable	94	97	75	84	30	84
3-CO_2H (c)	79	87	15	13	6	9	3	6
4-CO_2H (d)	77	87	31	46	3	12	9	9
3,5-I_2,4-OH (e)	0	0	0	1	1	4	4	3
3,5-Br_2,4-OH (f)	0	0	0	0	1	4	3	3
2-CF_3 (g)	65	34	1	0	83	83	32	71
3-CF_3 (h)	92	74	27	50	57	83	55	86
4-CF_3 (i)	98	90	83	94	81	93	68	77
3,5-F_2 (j)	95	78	8	18	75	88	61	94
3,5-Cl_2 (k)	56	1	0	9	33	72	63	90
2,6-Cl_2 (l)	63	59	1	0	15	21	62	24

Legend: 0-10% Good; 11-30% Moderate; >30% Poor

[a] Table entries represent percent fibril formation and thus inhibitor efficacy relative to WT-TTR fibril formation in the absence of inhibitor (assigned to be 100%): complete inhibition is equivalent to 0% fibril formation. Measurement error is ±5%. Blue, green, and yellow colors represent good (0−10% fibril formation), moderate (11−30% fibril formation), and poor (>31% fibril formation) inhibitors, respectively.

Table 2. Percent Oxime Ether Inhibitor Remaining at the Conclusion of the Acid-Mediated Fibril Formation Assay (72 h)[a]

	% inhibitor remaining			% inhibitor remaining	
inhibitor	without TTR	with TTR	inhibitor	without TTR	with TTR
1e	24	79	**4g**	79	84
1f	8	76	**4l**	85	81
2k	4	74	**5d**	80	83
3e	81	77	**5d***	0	76
3g	20	88	**5e**	89	100
4e	91	83	**5f**	78	98
4f	88	81			

[a] Inhibitor (7.2 μM) was incubated in the dark in the absence and presence of 3.6 μM WT-TTR (pH 4.4, 37 °C). The data for entry **5d*** were collected under identical conditions except the buffer was maintained at pH 7.2. Values were determined by comparing inhibitor analytical RP-HPLC peak areas at the end of the assay to those obtained at the start of the assay. Measurement error is ±4%.

their fibril formation inhibition properties. The 3,5-dihalo-4-hydroxybenzonitrile and the analogous aldehyde degradation products are potent inhibitors of TTR fibril formation at concentrations twice that of tetrameric TTR (Table S3). 3,5-Dichlorophenol also inhibits fibril formation by 86% at concentration (7.2 μM), twice that of tetrameric TTR (3.6 μM). However, none of the other degradation products (nitriles, phenols, or anilines) display appreciable activity. It is therefore reasonable to conclude that the efficacy of the vast majority of the amyloidogenesis inhibitors is due to the parent bis-aryloxime ether and not the degradative byproducts, providing the incentive to understand the mechanistic requirements for degradation and to stabilize these or related structures for medicinal chemistry purposes.

Analytical Ultracentrifugation Evaluation of TTR's Quaternary Structure under Amyloidogenic Conditions in the Presence of Inhibitor 8f. Both sedimentation velocity and equilibrium analytical ultracentrifugation experiments were used to evaluate the influence of inhibitor **8f** on TTR's quaternary structure under amyloidogenic conditions that typically dissociate the tetramer and make the monomer misassembly competent (72 h, pH 4.4, 37 °C). Oxime ether **8f** (7.2 μM) bound to WT-TTR (3.6 μM) was subjected to sedimentation velocity analysis at 50 000 rpm (Figure S2A) under these conditions, revealing that TTR remains tetrameric, sedimenting as a single species with an *S* value of 3.7, corresponding to a molecular mass of 48.4 ± 0.2 kDa. No tetrameric TTR was detectable in an identical experiment lacking inhibitor—only high molecular weight TTR aggregates were observed, consistent with the process of amyloidogenesis. Further scrutiny by sedimentation equilibrium analysis (17 000 rpm) reveal data that fit to a single ideal species model (Figure S2B; 52.1 ± 0.2 kDa), in good agreement with the calculated molecular mass of tetrameric WT-TTR·(**8f**)$_2$ (56 374 Da). Analysis of the molecular weight distribution across the cell as a function of concentration also indicated a single species with a molecular weight slightly above 50 kDa.

Selectivity of Oxime Ether Binding to TTR in Human Blood Plasma. To employ small molecules in clinical studies to test the amyloid hypothesis (the idea that the process of amyloidogenesis leads to neurotoxicity or tissue damage), they must bind selectively to TTR in blood plasma in the presence of all other plasma proteins. The binding stoichiometry of the most active oxime ethers to TTR in human blood plasma was evaluated using an antibody capture/HPLC method reported previously.[48] Briefly, the test compound is dissolved in human blood plasma at a concentration of 10.8 μM (approximately 2−3 times the plasma concentration of TTR). After incubation for 24 h (37 °C), TTR and any small molecules bound to it are immunocaptured using a polyclonal TTR antibody covalently linked to sepharose resin. The resin is washed, the TTR·(small molecule)$_{n<2}$ complex is dissociated at high pH, and the stoichiometry of the small molecule bound to TTR is then determined by reverse phase analytical HPLC employing standard curves to quantify the relative amounts of inhibitor and TTR (maximum inhibitor stoichiometry is 2, owing to TTR's two thyroxine binding sites). This method establishes a lower limit for inhibitor

Table 3. Bisaryloxime Ether Binding Stoichiometry to TTR in Human Blood Plasma[a]

Arylaldehyde Component	Aryloxyamine Component: H (1)	2-CO_2H (2)	3-CO_2H (3)	4-CO_2H (4)	2-CF_3 (5)	3-CF_3 (6)	3,5-Cl_2 (7)	3,5-F_2 (8)
3-CO_2H (c)					1.07	<0.5	0.56	<0.5
4-CO_2H (d)					1.38		0.78	<0.5
3,5-I_2,4-OH (e)	0.89	<0.5	<0.5	<0.5	1.71	1.02	0.55	1.83
3,5-Br_2-4-OH (f)	1.02	<0.5	<0.5	<0.5	1.86	1.17	0.69	1.42
2-CF_3 (g)			1.00	1.31				
3,5-F_2 (j)			<0.5					
3,5-Cl_2 (k)		<0.5	<0.5	0.53				
2,6-Cl_2 (l)			0.71	0.81				

Legend: >1.5 eq Excellent; 1.0-1.5 eq Good; 0.5-1.0 eq Moderate; <0.5 eq Poor

[a] TTR was treated with a variety of oxime ethers (10.8 μM) and the stoichiometry was determined by the antibody capture/HPLC method, which provides a minimum binding stoichiometry owing to wash-associated losses.[35,48]

binding stoichiometry because some of the inhibitor may be lost in the necessary wash steps following antibody capture.

The lower limits of the binding stoichiometry of bisaryloxime ethers displaying >90% amyloid inhibition (7.2 μM) to plasma TTR are presented in Table 3. Of the 31 compounds tested, 11 exhibit TTR binding stoichiometries exceeding 1.0, with three showing greater than 1.5 equiv bound. Oxime ethers exhibiting the highest binding stoichiometry are derived from aldehydes where one aromatic ring bears a thyroxine-like (e.g. 3,5-dihalo-4-hydroxy) substitution pattern. This result is very important, because it implies that incorporation of a 3,5-dihalo-4-hydroxy-substituted aryl ring imparts TTR plasma binding selectivity over the majority of other plasma proteins, including the thyroxine transport protein albumin, which has a concentration ~150 times greater than that of TTR.[25,68] However, these results do not address the potential of these compounds to bind to the primary thyroxine transport protein in blood, TBG, which is at a concentration roughly $^1/_{10}$ that of TTR. Hence, saturation of TBG's binding capacity would have little effect on the TTR binding selectivity results.[25] Several of the oxime ethers synthesized via automated procedures displaying binding stoichiometries exceeding 0.5 (**1e**, **5d**−**f**, **7e**, and **8e**−**f**) were also synthesized by conventional methods in milligram quantities and isolated, and their binding stoichiometry was reevaluated. In all cases the same results were obtained, demonstrating that the oxime ethers prepared via automation and those prepared by conventional methods were identical.

Crystal Structure of WT-TTR·(5d)$_2$. To elucidate the structural basis for amyloid inhibition by the bisaryloxime ethers, the cocrystal structures of several compounds displaying both potent aggregation inhibition and plasma selectivity were undertaken. The WT-TTR·(**5d**)$_2$ complex provided the best cocrystal structure data, with 1.53 Å resolution, and is presented herein (Figure 3 and Table S4). Despite the high-resolution data, the trifluoromethyl-substituted aromatic ring is visible only at less than 1σ contouring of the electron density omit maps, indicating relatively high flexibility in those regions. However, the side chain orientations and the shake/warp omit maps[69] yielded the final orientation and position of two molecules bound within the protein's central channel (one in each thyroid hormone binding pocket), approximately in their minimum energy conformations. Each hormone site contains two symmetry equivalent binding conformations due to the 2-fold symmetry axis bisecting the binding channel.

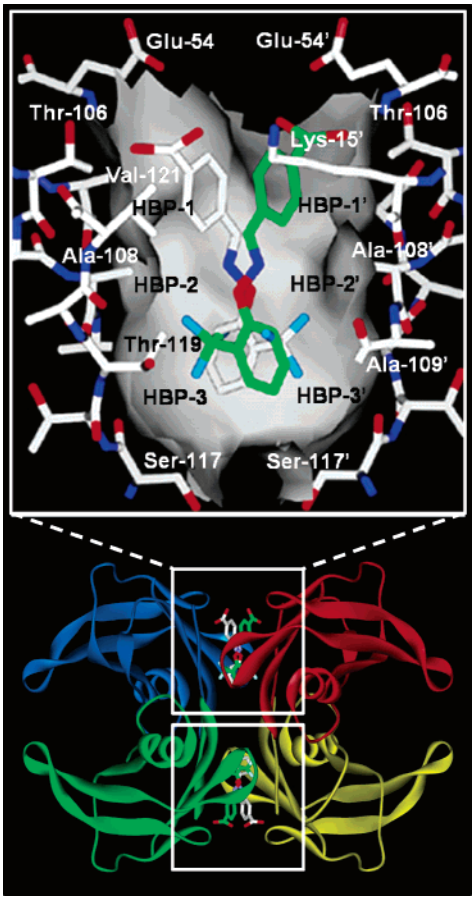

Figure 3. Ribbon diagram depiction of bisaryloxime ether **5d** bound to both of the WT-TTR thyroxine binding cavities (white boxes) based on X-ray crystallographic data. The expansion of one of the sites (top) shows **5d** in both of its symmetry-related binding modes (green and white), with the TTR binding site surface shown in gray. Key residues and halogen binding pockets (HBPs) are labeled; primed and unprimed residues or HBPs refer to two neighboring symmetry related monomers comprising the T_4 site. It appears that the carboxylate substituent in the outer binding pocket is making an electrostatic interaction with the ϵ-NH_3^+ group of Lys15.

Inhibitor **5d** resides in TTR in a "forward" binding mode, which refers to those inhibitors having a carboxylic acid substituted aromatic ring placed in the outer cavity to make favorable electrostatic interactions with Lys15.[42] The carboxyl group forms hydrogen bonds with the Thr106 (2.73 Å) and Lys15 residues; the Lys15 side chain contributes to both hydrophobic (ϵ-CH_2) and electrostatic (ϵ-NH_3^+, 3.3 Å) interactions with the inhibitor. Binding is also stabilized by both hydrophobic and van der Waals interactions, as the inhibitor is stacked between the hydrophobic side chains of Leu17, Leu17′, Ala108, Ala108′, Leu110, Leu110′, Thr119, Thr119′, Val121, and Val121′. The trifluoromethyl substituent occupies part of halogen binding pocket 3 (HBP-3) in the inner cavity. The inner cavity Ser117 hydroxyl groups orient away from the inhibitor, contributing additional hydrophobic interactions via their β-CH_2 substructures. The linker oxygen and nitrogen do not appear to make electrostatic interactions with TTR and therefore may not contribute greatly to its binding and

activity, consistent with the similar activities displayed by the oxime ethers and hydrazones and previous reports that stilbenes, diarylamines, and diaryl ethers are all active.[12,15,16,20,32−44] However, the conformation adopted by the linker appears to be crucial to orient the two aromatic rings.

Conclusions

X-ray crystallographic analysis of analogous bisaryloxime ethers and bisarylhydrazones show that they are isostructural. Of the 95-member oxime ether library synthesized, based on the hydrazone library activity, nearly one-third are excellent TTR amyloidogenesis inhibitors at a concentration of 7.2 μM, twice that of tetrameric WT-TTR (>90% inhibition at pH 4.4, over 72 h). The best inhibitors have one aromatic ring substituted with a carboxylic acid, while the other aryl ring bears halogens or a trifluoromethyl group. The oxime ethers prepared from arylaldehydes with a thyroxine-like substitution pattern also exhibit excellent activity and notable TTR plasma binding selectivity: several display binding stoichiometries exceeding 1.5 of 2. The oxime ethers not only selectively stabilize TTR's native state relative to the dissociative transition state, substantially slowing tetramer dissociation and amyloidosis, but by virtue of TTR binding, their degradation is notably slowed relative to just buffer, in cases where the bisaryloxime ethers exhibited lability. The potent activities and high plasma TTR binding selectivities displayed by the bisarylaldoxime ethers provide a wealth of knowledge from which to fashion future TTR amyloidogenesis inhibitors.

Experimental Section

General Synthetic Methods. Unless otherwise stated, all chemicals were purchased from commercial suppliers and used without further purification. Reaction progress was monitored by thin-layer chromatography on silica gel 60 F254 coated glass plates (EM Sciences) and/or by analytical RP-HPLC. All flash chromatography was performed using 230−400 mesh silica gel 60 (EM Sciences). NMR spectra were recorded on either Bruker 300, 400, 500, or 600 MHz spectrometers. Chemical shifts are reported in parts per million downfield from the internal standard Me_4Si (0.0 ppm) for $CDCl_3$ solutions, or in the case where the Me_4Si was not seen in the ^{13}C NMR spectra, calibration was done on the solvent peaks ($CDCl_3$ 77.16 ppm). For samples in DMSO-d_6, acetone-d_6, or CD_3OD, calibration was done on the solvent peak at 2.49, 2.05, and 3.31 ppm, respectively, for ^1H NMR and 39.52, 29.84, and 49.00 ppm, respectively, for ^{13}C NMR. Reverse-phase high-performance liquid chromatography (RP-HPLC) was carried out on a Waters 600 E multisolvent delivery system employing a Waters 486 tunable absorbance detector and a Waters 717 autosampler. A ThermoHypersil-Keystone Betabasic-18 column was used for analytical reverse phase HPLC analyses (model 71503-034630, 150 Å pore size, 3 μm particle size) and a Vydac C18 column for preparative HPLC (model 218TP1022, 300 Å pore size, 5 μm particle size, 22 mm i.d. by 250 mm). Solvent system A was 95:5 H_2O:CH_3CN with 0.25% trifluoroacetic acid (TFA) and solvent B was 5:95 H_2O:CH_3CN with 0.25% TFA; linear gradients were run from either 0:100, 80:20, or 60:40 A:B to 0:100 A:B. High-performance liquid chromatography−mass spectrometry (HPLC−MS) was performed on a Hewlett-Packard HPLC−MS equipped with a Zorbax SB-C18 (5 mm, 2.1 × 50 mm) column; solvent delivery was performed using a Gilson 215 liquid handler. All mass spectrometry data were collected at the Scripps Research Institute Center for Mass Spectrometry.

Representative Procedure for the Copper-Mediated Coupling of Phenylboronic Acids and *N*-Hydroxyphthalimide for the Preparation of Phenoxyamines (Method 1): Synthesis of 9. A 20 mL scintillation vial was charged with *N*-hydroxyphthalimide (163 mg, 1.0 mmol), copper(I) chloride (99 mg, 1.0 mmol), freshly activated 4 Å molecular sieves (~250 mg), and phenylboronic acid (244 mg, 2.0 mmol). 1,2-Dichloroethane (5 mL) was added followed by pyridine (90 μL, 1.1 mmol), resulting in a light brown suspension. The cap was loosely applied such that the reaction suspension was open to air and stirred at room temperature until completion as detected by analytical RP-HPLC (the mixture turned from brown to emerald green as the reaction proceeded). Upon completion (~48 h), the mixture was adsorbed onto silica gel and concentrated to a powder. Flash chromatographic purification over silica (25% EtOAc in hexanes) afforded *N*-phenoxyphthalimide **9** as a white solid (216 mg, 90%); see below for characterization data.

***N*-Phenoxyphthalimide (9).** Preparation of **9** was described above as the representative procedure (method 1): ^1H NMR (500 MHz, $CDCl_3$) δ 7.12−7.20 (m, 3H), 7.32−7.38 (m, 2H), 7.80−7.84 (m, 2H), 7.90−7.94 (m, 2H); ^{13}C NMR (125 MHz, $CDCl_3$) δ 114.4, 124.0, 128.8, 129.7, 134.9, 158.9, 162.9; MALDI−FTMS (DHB) 240.0656 *m/z* $[MH]^+$, $C_{14}H_{10}NO_3$, requires 240.0655.

***N*-(3-Trifluoromethylphenoxy)phthalimide (10).** 3-Trifluoromethylphenylboronic acid (380 mg, 2.0 mmol) was subjected to the representative coupling procedure with *N*-hydroxyphthalimide (NHP) as outlined above (method 1). Flash chromatographic purification over silica (40% EtOAc in hexanes) afforded **10** as a white solid (270 mg, 88%): ^1H NMR (500 MHz, $CDCl_3$) δ 7.34−7.38 (m, 1H), 7.40−7.45 (m, 2H), 7.47 (m, J = 0.9, 8.1 Hz, 1H), 7.82−7.87 (m, 2H), 7.92−7.97 (m, 2H); ^{13}C NMR (125 MHz, $CDCl_3$) δ 111.6, 117.8, 118.1, 121.4, 122.3, 124.2, 128.8, 130.5, 132.2, 135.1, 159.0, 162.8; LC−MS 309 *m/z* $[MH]^+$, $C_{15}H_9F_3NO_3$ requires 309.

***N*-(3,5-Dichlorophenoxy)phthalimide (11).** 3,5-Dichlorophenylboronic acid (382 mg, 2.0 mmol) was subjected to the representative coupling procedure with NHP as outlined above (method 1). Flash chromatographic purification over silica (50% CH_2Cl_2 in hexanes) afforded **11** as a white solid (139 mg, 45%): ^1H NMR (600 MHz, $CDCl_3$) δ 7.07 (m, 2H), 7.13−7.16 (m, 1H), 7.81−7.86 (m, 2H), 7.71−7.96 (m, 2H); ^{13}C NMR (150 MHz, $CDCl_3$) δ113.7, 124.2, 125.0, 128.8, 135.2, 135.9, 159.7, 162.5; LC−MS 276 *m/z* $[MH]^+$, $C_{14}H_8Cl_2NO_3$ requires 276.

***N*-(3,5-Difluorophenoxy)phthalimide (12).** 3,5-Difluorophenylboronic acid (316 mg, 2.0 mmol) was subjected to the representative coupling procedure with NHP as outlined above (method 1). Flash chromatographic purification over silica (10% CH_2Cl_2 in toluene) afforded **12** as a white solid (197 mg, 72%): ^1H NMR (600 MHz, $CDCl_3$) δ 6.58−6.63 (m, 1H), 6.68−6.73 (m, 2H), 7.82−7.87 (m, 2H), 7.92−7.97 (m, 2H); ^{13}C NMR (150 MHz, $CDCl_3$) δ 98.5 (m), 100.3 (t, J_{C-F}=25.3 Hz), 124.4, 128.7, 135.4, 160.5 (t, J_{C-F} = 13.8 Hz), 162.6, 163.6 (dd, J_{C-F} = 13.8, 249 Hz); MALDI−FTMS (DHB) 276.0456 *m/z* $[MH]^+$, $C_{14}H_8F_2NO_3$ requires 276.0467.

***N*-(3-Methoxycarbonylphenoxy)phthalimide (13).** 3-Methoxycarbonylphenylboronic acid was subjected to similar coupling procedures with NHP as outlined above (method 1). A 100 mL round-bottom flask was charged with *N*-hydroxyphthalimide (2.19 g, 13.4 mmol), copper(I) chloride (1.34 g, 13.5 mmol), freshly activated 4 Å molecular sieves (~5 g), and 3-methoxycarbonylphenylboronic acid (4.79 g, 26.6 mmol). 1,2-Dichloroethane (60 mL) was added followed by pyridine (1.20 mL, 14.8 mmol), and the reaction suspension was stirred in an air atmosphere at room temperature. After 4 days, the mixture was adsorbed onto silica gel and concentrated to a powder. Flash chromatographic purification over silica (33−50% gradient EtOAc in hexanes) afforded **13** as a white solid (1.85 g, 46%): ^1H NMR (500 MHz, $CDCl_3$) δ 3.90 (s, 3H), 7.38−7.41 (ddd, J = 1.0, 2.5, 8.3 Hz, 1H), 7.44 (t, J = 8.3 Hz, 1H), 7.78 (dd, J = 1.0, 2.5 Hz, 1H), 7.82−7.86 (m, 3H), 7.92−7.96 (m, 2H); ^{13}C NMR (125 MHz, $CDCl_3$) δ 52.5, 115.0, 119.3, 124.3,

125.9, 129.0, 130.0, 132.1, 135.2, 159.0, 163.0, 166.2; ESI-MS 298 *m/z* $[MH]^+$, $C_{16}H_{12}NO_5$ requires 298.

Representative Procedure for the Hydrazinolysis of *N*-Aryloxyphthalimides to Corresponding *O*-Arylhydroxylamines (Method 1A): Synthesis of Compound 1. Hydrazine monohydrate (0.401 mL, 8.2 mmol) was added slowly to a solution of *N*-phenoxyphthalimide **9** (652 mg, 2.73 mmol) in 10% MeOH in $CHCl_3$ (25 mL) and the reaction was stirred at room temperature. Upon completion (TLC monitoring, 12 h) a white precipitate appeared (the phthalizine) in a colorless reaction solution. The reaction mixture was passed through a plug of silica gel, washing with 30% EtOAc in hexane. Removal of the EtOAc/hexanes produced a slightly pale yellow oil, which upon Kugelrohr distillation from K_2CO_3 (<10 mg) provided pure phenoxyamine **1** as a clear, colorless oil (238 mg, 80%) (see below for characterization data). Alternatively, after removal of the EtOAc/hexanes, the yellow oil was dissolved in Et_2O and cooled to 0 °C. After 10 min at 0 °C, 4 N HCl in dioxane was added dropwise until pH 3 was reached. The resulting white solid was filtered and washed with Et_2O (2 × 10 mL) to afford **1** as the pure HCl salt (306 mg, 77%).

***O*-Phenylhydroxylamine Hydrochloride (1).** Preparation of **1** was described above as the representative procedure (method 1A): ^{1}H NMR (400 MHz, CD_3OD) δ 6.84−6.89 (m, 1H), 7.03−7.09 (m, 2H), 7.19−7.25 (m, 2H); ^{13}C NMR (100 MHz, CD_3OD) δ 114.1, 121.6, 130.3, 163.1; LC−MS 110 *m/z* $[MH]^+$, C_6H_8NO requires 110.

***O*-(3-Trifluoromethylphenyl)hydroxylamine (6).** *N*-(3-Trifluoromethylphenoxy)phthalimide **10** (1.12 g, 3.65 mmol) was subjected to the representative hydrazinolysis reaction as described above (method 1A). Distillation (85 °C/6 mm) provided pure **6** as a clear colorless liquid (582 mg, 90%): ^{1}H NMR (500 MHz, $CDCl_3$) δ 6.00 (s, 2H), 7.19−7.21 (m, 1H), 7.30 (dd, J = 8.4, 2.6 Hz, 1H), 7.38 (t, J = 8.1 Hz, 1H), 7.45−7.47 (m, 1H); ^{13}C NMR (125 MHz, $CDCl_3$) δ 110.4, 117.2, 117.9, 130.9, 162.1; LC−MS 178 *m/z* $[MH]^+$, $C_7H_7F_3NO$ requires 178.

***O*-(3,5-Dichlorophenyl)hydroxylamine (7).** *N*-(3,5-Dichlorophenoxy)phthalimide **11** (711 mg, 2.31 mmol) was subjected to the representative hydrazinolysis reaction as described above (method 1A). Elution of the reaction mixture through the silica gel plug resulted in solidification of free base **7** as a white solid (378 mg, 92%): ^{1}H NMR (600 MHz, $CDCl_3$) δ 5.91 (s, 2H), 6.91−6.93 (m, 1H). 7.06−7.09 (m, 2H); ^{13}C NMR (150 MHz, $CDCl_3$) δ 112.9, 121.9, 135.9, 163.2; LC−MS 179 *m/z* $[MH]^+$, $C_6H_6Cl_2NO$ requires 179.

***O*-(3,5-Diflourophenyl)hydroxylamine Hydrochloride (8).** *N*-(3,5-Difluorophenoxy)phthalimide **12** (1.74 g, 6.31 mmol) was subjected to the representative hydrazinolysis reaction as described above (method 1A). Precipitation of the HCl salt afforded **8** as a white solid (980 mg, 86%): ^{1}H NMR (600 MHz, CD_3OD) δ 6.83−6.90 (m, 3H); ^{13}C NMR (150 MHz, CD_3OD) δ 99.3 (dd, J_{C-F} = 8.0, 24.9 Hz), 101.1 (t, J_{C-F} = 26.4 Hz), 160.0, 165.8 (dd, J_{C-F} = 15, 248 Hz); LC−MS 146 *m/z* $[MH]^+$, $C_6H_6F_2NO$ requires 146.

***O*-(3-Methoxycarbonylphenyl)hydroxylamine (14).** *N*-(3-Methoxycarbonylphenoxy)phthalimide **13** (271 mg, 0.912 mmol) was subjected to the representative hydrazinolysis reaction as described above (method 1A) to afford **14** as a pale yellow syrup (146 mg, 96%): ^{1}H NMR (500 MHz, $CDCl_3$) δ 3.91 (s, 3H), 5.92 (s, 2H), 7.29−7.32 (m, 1H), 7.33 (t, J = 6.9 Hz, 1H), 7.63 (dt, J = 1.8, 6.9 Hz, 1H), 7.82−7.84 (m, 1H); ^{13}C NMR (125 MHz, $CDCl_3$) δ 52.3, 114.2, 118.1, 122.5, 129.3, 131.4, 161.4, 167.1; GC−MS167 *m/z* $[M]^+$, $C_8H_9NO_3$ requires 167, 152 *m/z* $[M - NH]^+$, $C_8H_8O_3$ requires 152.

***O*-(3-Carboxyphenyl)hydroxylamine (3).** $LiOH{\cdot}H_2O$ (91.0 mg, 2.17 mmol) was added to a solution of *O*-(3-methoxycarbonylphenyl)hydroxylamine **14** (90.4 mg, 0.541 mmol) in a 3/1/1 mL mixture of THF/MeOH/H_2O and the reaction was stirred at room temperature. After 24 h the reaction was diluted with H_2O (50 mL), acidified to pH ∼3−4 with 0.5 N HCl, and extracted with EtOAc (3 × 25 mL). The combined organics were washed with H_2O (25 mL) and brine (25 mL), dried over Na_2SO_4, filtered, and concentrated to afford **3** as a white solid (78.7 mg, 95%): ^{1}H NMR (500 MHz, DMSO-d_6) δ 7.01 (s, 2H), 7.24 (ddd, J = 1.4, 2.8, 8.3 Hz, 1H), 7.34 (t, J = 7.8 Hz, 1H), 7.46 (dt, J = 1.4, 7.3 Hz, 1H), 7.68 (dd, J = 1.4, 2.8 Hz, 1H); ^{13}C NMR (125 MHz, DMSO-d_6) δ 113.5, 117.8, 121.3, 129.2, 131.8, 161.7, 167.3; ESI-MS 162 *m/z* $[M - H^+]^-$, $C_7H_6NO_3$ requires 162.

Ethyl *N*-(2-trifluoromethylphenoxy)acetimidate (15) was prepared using a procedure adapted from Miyazawa et al.[58] ^{t}BuOK (0.78 g, 6.7 mmol) was added to a stirring solution of ethyl *N*-hydroxyacetimidate (1.00 g, 6.06 mmol) in anhydrous DMF (6 mL) at 0 °C under an Ar atmosphere. After ^{t}BuOK addition was completed, the reaction was stirred at room temperature. After 30 min, 2-fluorobenzotrifluoride (1.29 mL, 6.06 mmol) was added and the reaction was heated at 80 °C for 2 h. Upon cooling the reaction mixture was diluted with ice water (100 mL) and extracted with EtOAc (3 × 40 mL). The combined organic layers were washed with brine (2 × 50 mL), dried with $MgSO_4$, and concentrated to afford a dark oil. Flash chromatographic purification over silica (10% EtOAc in hexanes) afforded **15** as a clear liquid (1.33 g, 89%): ^{1}H NMR (500 MHz, $CDCl_3$) δ 1.36 (t, J = 7.1 Hz, 3H), 2.15 (s, 3H), 4.20 (q, J = 7.1 Hz, 2H), 6.99 (apparent t, J = 7.5 Hz, 1H), 7.47 (apparent dt, J = 7.9 Hz, 1H), 7.52−7.57 (m, 2H); ^{13}C NMR (125 MHz, $CDCl_3$) δ 14.3, 14.5, 63.2, 114.2, 116.2 (q, J_{C-F} = 31 Hz), 120.3, 123.7 (q, J_{C-F} = 272 Hz), 126.4 (q, J_{C-F} = 4.8 Hz), 133.2, 157.2 (q, J_{C-F} = 1.9 Hz), 167.1; LC−MS 248 *m/z* $[MH]^+$, $C_{11}H_{13}F_3NO_2$ requires 248.

***O*-(2-Trifluoromethylphenyl)hydroxylamine hydrochloride (5)** was prepared using a procedure adapted from Miyazawa et al.[58] $HClO_4$ (70%, 12 mL) was added dropwise to a solution of **15** (4.14 g, 16.7 mmol) in 1,4-dioxane (19 mL) at 0 °C and then the reaction was stirred at room temperature overnight. The reaction mixture was then poured into ice water (150 mL) and adjusted to pH 13 with solid NaOH pellets. The aqueous layer was extracted with EtOAc (3 × 150 mL), and the combined organics were washed with brine (2 × 75 mL), dried over $MgSO_4$, and concentrated to afford a dark residue. Flash chromatographic purification over silica (15% EtOAc in hexanes) followed by precipitation of the HCl salt, as described above for other aryloxyamines, afforded **5** as a white solid (3.42 g, 96%): ^{1}H NMR (600 MHz, CD_3OD) δ 7.37−7.41 (m, 1H), 7.48−7.51 (m, 1H), 7.76−7.79 (m, 2H); ^{13}C NMR (150 MHz, CD_3OD) δ 114.6, 125.0, 126.3, 127.6 (q, J_{C-F} = 5.7 Hz), 128.3 134.5; LC−MS 178 *m/z* $[MH]^+$, $C_7H_7F_3NO$ requires 178.

Library Synthesis for Aryloxyamine 1 and 5−8 Based Oxime Ethers. Libraries were prepared in a single compound per well format. Stock solutions of all aldehydes (0.5 M) and aryloxyamines (0.4 M) were prepared in DMSO. A Gilson 215 Liquid Handler equipped with a 1 mL syringe, 1.1 mL tubing, and a 13 mm i.d. probe was used to distribute all solutions into a 96 well (2 mL volume) polypropylene plate at a rate of 0.3 mL/min. To make 0.5 mL of a 0.1 M solution of each oxime ether, 100 μL (0.05 mmol, 1 equiv) of aldehyde, 156 μL (0.63 mmol, 1.25 equiv) of aryloxyamine, and 244 μL of 0.164 M acetic acid were distributed to each well of the plate. The plate was covered and agitated for 24 h at room temperature using a dual action shaker. The reactions were diluted to 720 μM in DMSO and analyzed by LC−MS to determine yield, purity, and identity. Compounds were stored frozen at −20 °C after synthesis.

Reaction yield was determined using the integrated value of aldehyde that remained in the reaction mixture. Calibration curves of all aldehydes were made and the yield of each oxime ether was calculated by assuming all the aldehyde that reacted quantitatively formed oxime ether; i.e., if 5% of aldehyde remained in the reaction mixture the yield of oxime ether would be 95%. Yields ranged from 98 to 100% and purity was >95% in all wells.

Representative Procedure for the Coupling of *O*-(3-Carboxyphenyl)hydroxylamine 3 to Arylaldehydes a−l (Method 2). To a stirring solution of *O*-(3-carboxyphenyl)-hydroxylamine **3** (∼0.2 mmol, 1 equiv) in 1,4-dioxane (3.0 mL) was added the aldehyde (1 equiv) followed by 1 drop of 0.5 N HCl, then the reaction was stirred at room temperature. Upon completion as determined by reverse phase HPLC (3−18 h),

the reaction was diluted with H_2O (15 mL) and the precipitate filtered, washed with H_2O, collected, and dried in vacuo. Refer to the Supporting Information for specific synthetic details and characterization data for inhibitors **3b**−**l** analogous to that reported for **3a** below.

Benzaldehyde *O*-(3-Carboxyphenyl)oxime (3a). Benzaldehyde (21.0 μL, 0.207 mmol) was subjected to the representative coupling procedure with **3** (31.8 mg, 0.208 mmol) as outlined above (method 2), yielding **3a** as a white solid (29.0 mg, 58%): ^{1}H NMR (500 MHz, 1:1 CD_3OD:DMSO-d_6) δ 7.39−7.45 (m, 5H), 7.59−7.64 (m, 1H), 7.71−7.78 (m, 3H), 8.58 (s, 1H); ^{13}C NMR (125 MHz, DMSO-d_6) δ 114.5, 118.8, 123.3, 127.7, 129.1, 129.3, 130.8, 131.1, 132.3, 153.3, 158.9, 166.9; MALDI−FTMS (DHB) 242.0812 *m/z* $[MH]^+$, $C_{14}H_{12}NO_3$ requires 242.0812; RP-HPLC 98% pure.

Benzyl 2-Fluorobenzoate (16). Benzyl alcohol (2.60 mL, 25.1 mmol) was added slowly to a stirring solution of 2-fluorobenzoic acid (2.92 g, 20.8 mmol), 4-(dimethylamino)pyridine (251 mg, 2.05 mmol), and 1,3-dicyclohexylcarbodiimide (5.16 g, 25.0 mmol) in anhydrous CH_2Cl_2 at room temperature under an Ar atmosphere. After 18 h the precipitate was filtered off and washed with CH_2Cl_2, and the filtrate was concentrated with silica to a powder. Flash chromatographic purification over silica (10% to 20% gradient EtOAc in hexanes) afforded **16** as a clear, colorless liquid (4.20 g, 88%): ^{1}H NMR (500 MHz, $CDCl_3$) δ 5.39 (s, 2H), 7.14 (ddd, J = 1.1, 8.4, 9.5 Hz, 1H), 7.20 (dt, J = 1.1, 7.7 Hz, 1H), 7.31−7.36 (m, 1H), 7.37−7.41 (m, 2H), 7.44−7.48 (m, 2H), 7.49−7.55 (m, 1H), 7.96 (dt, J = 1.8, 7.3 Hz); ^{13}C NMR (125 MHz, $CDCl_3$) δ 66.93, 117.0 (d, J_{C-F} = 22.1 Hz), 118.7 (d, J_{C-F} = 9.6 Hz), 124.0 (d, J_{C-F} = 3.8 Hz), 128.1, 128.2, 128.6, 132.2, 134.6 (d, J_{C-F} = 9.6 Hz), 135.7, 162.1 (d, J_{C-F} = 260 Hz), 164.2 (d, J_{C-F} = 3.8 Hz); GC−MS230 *m/z* $[M]^+$, $C_{14}H_{11}FO_2$ requires 230.

Benzyl 4-Fluorobenzoate (17). Benzyl alcohol (4.05 mL, 39.1 mmol) was added slowly to a stirring solution of 4-fluorobenzoic acid (5.00 g, 35.7 mmol), 4-(dimethylamino)pyridine (432 mg, 3.53 mmol), and 1,3-dicyclohexylcarbodiimide (8.15 g, 39.5 mmol) in anhydrous CH_2Cl_2 at room temperature under an argon atmosphere. After 18 h the reaction was worked up according to procedures as outlined for the synthesis of **16**. Flash chromatographic purification over silica (10% EtOAc in hexanes) afforded **17** as a clear, colorless liquid (7.75 g, 94%): ^{1}H NMR (500 MHz, $CDCl_3$) δ 5.35 (s, 2H), 7.06−14 (m, 2H), 7.32−7.41 (m, 3H), 7.41−7.47 (m, 2H), 8.06−8.12 (m, 2H); ^{13}C NMR (125 MHz, $CDCl_3$) δ 66.84, 115.5 (d, J_{C-F} = 22.0 Hz), 126.4 (d, J_{C-F} = 2.9 Hz), 128.2, 128.3, 128.6, 132.3 (d, J_{C-F} = 9.6 Hz), 135.9, 165.5, 165.8 (d, J_{C-F} = 253 Hz); GC−MS 230 *m/z* $[M]^+$, $C_{14}H_{11}FO_2$ requires 230.

Ethyl *N*-(2-Benzyloxycarbonylphenoxy)acetimidate (18). To a stirring solution of ethyl *N*-hydroxyacetimidate (2.06 g, 20.0 mmol) in anhydrous DMF (60 mL) under Ar was added ^{t}BuOK (2.21 g, 19.7 mmol) all at once. After 30 min benzyl 2-fluorobenzoate **16** (4.13 g, 17.9 mmol) was added as a solution in DMF (20 mL) and the reaction was stirred at room temperature. After 3 h the reaction was diluted with H_2O (400 mL) and extracted with EtOAc (3 × 100 mL), and the combined organics were washed with H_2O (3 × 50 mL) and brine (50 mL), dried over Na_2SO_4, filtered, and concentrated. Flash chromatographic purification over silica (5−10% gradient EtOAc in hexanes) afforded **18** as a clear syrup (3.61 g, 64%): ^{1}H NMR (500 MHz, $CDCl_3$) δ 1.34 (t, J = 7.0 Hz, 3H), 2.00 (s, 3H), 4.18 (q, J = 7.0 Hz, 2H), 5.34 (s, 2H), 6.96 (dt, J = 1.1, 7.7 Hz, 1H), 7.30−7.35 (m, 1H), 7.35−7.39 (m, 2H), 7.42−7.48 (m, 3H), 7.55 (dd, J = 1.1, 8.4 Hz, 1H), 7.90 (dd, J = 1.8, 7.7 Hz, 1H); ^{13}C NMR (125 MHz, $CDCl_3$) δ 14.4, 14.5, 63.1, 66.6, 114.5, 117.0, 120.4, 128.2, 128.4, 128.5, 131.7, 133.8, 136.1, 159.5, 165.8, 166.7; GC−MS 313 *m/z* $[M]^+$, $C_{18}H_{19}NO_4$ requires 313, 228 *m/z* $[M - 85]^+$, benzyl 2-hydroxybenzoate $C_{14}H_{12}O_3$ requires 228.

Ethyl *N*-(4-Benzyloxycarbonylphenoxy)acetimidate (19). To a stirring solution of ethyl *N*-hydroxyacetimidate (3.79 g, 36.8 mmol) in anhydrous DMF (150 mL) under Ar was added ^{t}BuOK (4.09 g, 36.4 mmol) all at once. After 40 min benzyl 4-fluorobenzoate **17** (7.63 g, 17.9 mmol) was added and the reaction was stirred at room temperature. After 4 h the reaction was diluted with H_2O (500 mL) and extracted with EtOAc (4 × 100 mL), and the combined organics were washed with H_2O (2 × 100 mL), dried over Na_2SO_4, filtered, and concentrated. Flash chromatographic purification over silica (5−10% gradient EtOAc in hexanes) afforded **19** as a clear syrup (6.02 g, 58%): ^{1}H NMR (500 MHz, $CDCl_3$) δ 1.36 (t, J = 7.0 Hz, 3H), 2.12 (s, 3H), 4.20 (q, J = 7.0 Hz, 2H), 5.34 (s, 2H), 7.15−7.19 (m, 2H), 7.31−7.35 (m, 2H), 7.36−7.41 (m, 2H), 7.42−7.36 (m, 2H), 8.00−8.14 (m, 2H); ^{13}C NMR (125 MHz, $CDCl_3$) δ 14.3, 14.4, 63.1, 66.4, 113.4, 122.9, 128.1, 128.1, 128.6, 131.5, 136.3, 163.5, 166.3, 166.4; GC−MS 228 *m/z* $[M - 85]^+$, benzyl 4-hydroxybenzoate $C_{14}H_{12}O_3$ requires 228.

Ethyl *N*-(2-Carboxyphenoxy)acetimidate (20). LiOH·H_2O (431 mg, 10.3 mmol) was added to a solution of ethyl-*N*-(2-benzyloxycarbonylphenoxy)acetimidate **18** (802 mg, 2.56 mmol) in a 9/3/3 mL mixture of THF/MeOH/H_2O and the reaction was stirred at room temperature. After 6 h the reaction was diluted with H_2O (100 mL), washed with CH_2Cl_2 (4 × 30 mL), acidified to pH ∼5.0−5.5 with 0.5 N HCl, and extracted with EtOAc (4 × 30 mL). The combined organics were washed with H_2O (30 mL) and brine (30 mL), dried over Na_2SO_4, filtered, and concentrated to afford **20** as a white solid (459 mg, 80%): ^{1}H NMR (500 MHz, acetone-d_6) δ 1.34 (t, J = 6.9 Hz, 3H), 2.18 (s, 3H), 4.20 (q, J = 6.9 Hz, 2H), 7.02 (ddd, J = 0.9, 7.3, 7.8 Hz, 1H), 7.51 (ddd, J = 1.8, 7.3, 8.7 Hz, 1H), 7.60 (dd, J = 0.9, 8.7 Hz, 1H), 7.86 (dd, J = 1.8, 7.8 Hz, 1H); ^{13}C NMR (125 MHz, acetone-d_6) δ 14.6, 14.7, 63.8, 115.2, 118.5, 121.3, 132.4, 134.5, 160.2, 166.8, 167.4; ESI-MS 224 *m/z* $[MH]^+$, $C_{11}H_{14}NO_4$ requires 224.

Ethyl *N*-(4-Carboxyphenoxy)acetimidate (21). LiOH·H_2O (550 mg, 13.1 mmol) was added to a solution of ethyl *N*-(4-benzyloxycarbonylphenoxy)acetimidate **19** (1.04 g, 3.32 mmol) in a 9/3/3 mL mixture of THF/MeOH/H_2O and the reaction was stirred at room temperature. After 24 h the reaction was diluted with H_2O (100 mL), washed with CH_2Cl_2 (4 × 30 mL), acidified to pH ∼5.0−5.5 with 0.5 N HCl, and extracted with EtOAc (3 × 30 mL). The combined organics were washed with H_2O (30 mL) and brine (30 mL), dried over Na_2SO_4, filtered, and concentrated to afford **21** as a white crystalline solid (698 mg, 94%): ^{1}H NMR (500 MHz, $CDCl_3$) δ 1.37 (t, J = 6.9 Hz, 3H), 2.14 (s, 3H), 4.22 (q, J = 6.9 Hz, 2H), 7.18−7.22 (m, 2H), 8.04−8.08 (m, 2H); ^{13}C NMR (125 MHz, $CDCl_3$) δ 14.5, 14.6, 63.3, 113.7, 122.1, 132.3, 164.2, 166.7, 172.0; ESI-MS 224 *m/z* $[MH]^+$, $C_{11}H_{14}NO_4$ requires 224.

Representative Procedure for the Coupling of Ethyl *N*-(2-Carboxyphenoxy)acetimidate 20 or Ethyl *N*-(4-Carboxyphenoxy)acetimidate 21 to Arylaldehydes a−l Yielding Oxime Ethers 2a−l and 4a−l, Respectively (Method 3). To a solution of acetimidate **20** or **21** (∼0.1−0.3 mmol, 1 equiv) and aldehyde (∼0.1−0.3 mmol, 1 equiv) in 1,4-dioxane (2.0 mL) was added 70% $HClO_4$ (0.9 equiv) and the reaction was stirred at room temperature. Upon completion as determined by reverse phase HPLC (2−6 h), the reaction was diluted with H_2O (20 mL) and the precipitate filtered, washed with H_2O, collected, and dried in vacuo. Refer to the Supporting Information for specific synthetic details and characterization data of inhibitors **2c**−**l** and **4b**−**l** analogous to **2a** as shown below.

Benzaldehyde-*O*-(2-carboxyphenyl)oxime (2a). $HClO_4$ (70%, 14.0 μL, 0.163 mmol), benzaldehyde (18.0 mL, 0.177 mmol), and **20** (39.0 mg, 0.175 mmol) were subjected to the representative coupling procedure as outlined above (method 3), yielding **2a** as a white solid (26.1 mg, 62%): ^{1}H NMR (500 MHz, acetone-d_6) δ 7.15 (dt, J = 0.9, 7.8 Hz, 1H), 7.48−7.55 (m, 3H), 7.59 (dt, J = 1.8, 7.8 Hz, 1H), 7.71 (d, J = 8.2 Hz, 1H), 7.83−7.89 (m, 3H), 8.66 (s, 1H), 10.8−11.5 (broad s, 1H); ^{13}C NMR (125 MHz, DMSO-d_6) δ 115.7, 119.7, 122.1, 127.8, 129.0, 130.8, 130.9, 131.1, 133.1, 153.4, 157.7, 166.8; MALDI−FTMS (DHB) 242.0811 *m/z* $[MH]^+$, $C_{14}H_{12}NO_3$ requires 242.0812; RP-HPLC >99% pure.

Fibril Formation Assay. Wild type TTR was purified from an *Escherichia coli* expression system as described previously.[70] Disposable cuvettes (Fisher #14 385 938) were charged

with 495 μL of a 0.4 mg/mL stock of TTR (7.2 μM) in 10 mM phosphate (pH 7.2), 100 mM KCl, 1 mM EDTA, and 0.2% NaN_3. A 5 μL portion of the inhibitors in DMSO (1.44 mM) was added to the TTR solutions and the samples were incubated for 30 min at 37 °C. The pH was then lowered to 4.4 by addition of 0.5 mL of 200 mM acetate buffer (pH 4.2, 100 mM KCl, 1 mM EDTA, 0.2% NaN_3) to each cuvette. The cuvettes were left undisturbed for 72 h at 37 °C and then vortexed to evenly distribute any precipitate throughout the sample. The turbidity was measured on a Hewlett-Packard model 8453 UV−vis spectrophotometer at 350 and 400, or 500 nm. All samples were performed in duplicate or triplicate, and results reported are representative examples of at least three analyses.

Partitioning of Oxime Ether Inhibitors into TTR in Human Blood Plasma. The procedure for the antibody capture approach to evaluate inhibitor binding stoichiometry to TTR in human blood plasma has been described in detail elsewhere.[48] Briefly, human blood plasma (1.5 mL) was added to a 2 mL Eppendorf tube, followed by 7.5 μL of a 2.16 mM DMSO solution of test compound. This solution was incubated at 37 °C for 24 h, at which point 187 μL of a 1:1 (v:v) slurry of unfunctionalized Sepharose resin in 10 mM Tris, (pH 8.0), 140 mM NaCl, 0.025% NaN_3 (TSA) was added. This was incubated for another hour at 4 °C and then centrifuged. The supernatant was divided into three aliquots of 400 μL, and each aliquot was added to 200 μL of a 1:1 slurry of Sepharose resin conjugated to an *anti*-TTR antibody in TSA. After 20 min of gentle agitation at 4 °C, the samples were centrifuged, the supernatant was removed, and the *anti*-TTR resin was washed with 1 mL of TSA/0.05% Saponin (3 × 10 min) and then 1 mL of TSA (2 × 10 min) at 4 °C. After centrifugation and removal of the supernatant, 155 μL of 100 mM triethylamine (pH 11.5) was added to dissociate the TTR and bound test compound from the resin-bound antibodies. After 30 min, the suspension was centrifuged and 145 μL of the supernatant, containing TTR and test compound, was removed. The supernatant (135 μL) was then injected onto an HPLC to determine the stoichiometry of small molecule binding to TTR. Under HPLC conditions, the test compound−TTR complex dissociates and the small molecule and protein can be separated. HPLC conditions: Keystone 3 cm C18 reverse phase column using either a 20−100% or 40−100% solvent B gradient over 8 min (solvent A, 95:5 H_2O:CH_3CN, 0.25% TFA; solvent B, 5:95H_2O:CH_3CN, 0.25% TFA). The test compound and TTR quantification can be achieved by comparing the chromatogram integrated peak areas to standard curves; the ratio of the amount of test compound to TTR yields the binding stoichiometry.[48]

Analytical Ultracentrifugation: Sedimentation Velocity Profile Analysis of TTR under Fibril Formation Conditions in the Presence of Oxime Ether Based Inhibitors. Sedimentation analyses were performed at pH 4.4 on samples used previously in the fibril formation assay (see above). The sedimentation properties of recombinant WT-TTR solutions in the presence and absence of oxime ether inhibitor **8f** were analyzed on a temperature-controlled Beckman XL-I analytical ultracentrifuge equipped with an An60Ti rotor and photoelectric scanner. Data were collected at speeds of 3000 and 50 000 rpm in continuous mode at 20 °C, employing a step size of 0.001 cm, with detection at 280 nm.

A direct boundary fitting approach was applied to evaluate the sedimentation velocity data derived from a 3.6 μM TTR solution incubated with 7.2 μM of **8f** at pH 4.4. The program Svedberg was used to fit multiple concentration vs radial position data sets simultaneously to yield approximate solutions to the Lamm equation.[71] The fitting algorithm yields the sedimentation coefficient and diffusion coefficient that afford the molecular weight using the following equation:[71]

$$\mathrm{MW} = \frac{sRT}{D(1-\bar{\nu}\rho)}$$

where MW is the molecular weight, s is the sedimentation coefficient (in svedbergs, 10^{-13} s), R is the universal gas constant (8.314×10^7 erg/mol), $\bar{\nu}$ is the partial specific volume (cm^3/g), and ρ is the solvent density (g/cm^3). The buffer density D (1.00848 g/cm^3) was calculated from tabulated data and the partial specific volume of WT-TTR (0.7346 cm^3/g) was calculated from its amino acid composition.

Analytical Ultracentrifugation: Sedimentation Equilibrium Analysis of TTR under Fibril Formation Conditions in the Presence of Oxime Ether Based Inhibitors. Sedimentation analyses were performed at pH 4.4 on samples used previously in the fibril formation assay (see above). Sedimentation equilibrium measurements were made by loading 120−140 μL of a solution of TTR (3.6 μM) and oxime ether **8f** (7.2 μM) into a double sector cell, equipped with a 12-mm Epon centerpiece and sapphire or quartz windows. Data were collected initially at rotor speeds of 3000 rpm to ensure the absence of large molecular weight oligomers, which would sediment out first, and then at 17 000 rpm to establish an equilibrium across the cell. The sedimentation profiles, monitored between 285 and 290 nm at 3 h intervals, were overlaid to establish that equilibrium had been achieved. Data analysis was performed using a nonlinear least-squares analysis in the Origin software package provided by Beckman. The data were fit by several different models, including a single ideal species and several multiple species models, to identify the simplest model that best fit the data. The following equation, corresponding to a single ideal species model, fit the data best on the basis of the small differences between the theoretical data and the experimental data:[71]

$$A_r = \exp\left[\ln(A_o) + M\omega^2\left(1-\frac{\bar{\nu}\rho}{RT}\right)(x^2 - x^2{}_o)\right] + E$$

where A_r is the absorbance at radius x, A_o is the absorbance at a reference radius x_o (usually the meniscus), $\bar{\nu}$ is the partial specific volume of the protein, ρ is the density of the solvent (g/cm^3), ω is the angular velocity of the rotor (rad/s), E is the baseline error correction factor, M is the molecular weight, and R is the universal gas constant. The differences between the experimental data points and the fitted data points (the residuals) were randomly distributed and small in magnitude (when the data was fit to a single ideal species model (TTR tetramer). Other models did not fit the data well as discerned by the nonrandom distribution of residuals across the cell.

WT-TTR·(5d)$_2$ Crystallization and X-ray Data Collection. WT-TTR crystals were obtained from 7 mg/mL protein solutions (100 mM KCl, 1 mM EDTA, 10 mM sodium phosphate, pH 7.0, 0.35−0.50 M ammonium sulfate) equilibrated against 2 M ammonium sulfate in hanging drop experiments. The TTR·(**5d**)$_2$ complexes were prepared from WT-TTR crystals soaked for more than 3 weeks with a 10-fold molar excess of inhibitor **5d**. The crystals were placed in paratone oil as a cryoprotectant and cooled to 100 K. Data collection was performed using a Quantum-4 detector with a monochromatic high-energy source of 14-BM-C, BIOCARS, Advance Photon Source. Crystals of TTR·(**5d**)$_2$ are isomorphous with the apo-TTR crystal form with unit cell dimensions close to $a = 43$ Å, $b = 85$ Å, and $c = 66$ Å (space group $P2_12_12$ with two monomers in the asymmetric unit). Data were reduced with DENZO and SCALEPAC.[72]

WT-TTR·(5d)$_2$ Crystal Structure Determination and Refinement. The protein atomic coordinates for apo-TTR from the Protein Data Bank (accession number 1BMZ) were refined by molecular dynamics and energy minimization protocols of the CNS against the 1.53 Å data set of TTR·(**5d**)$_2$.[73] The resulting difference Fourier maps showed significant electron densities in the outer binding cavity; however, inhibitor electron density in the inner cavity was only visible when the electron density maps were contoured below 1σ, presumably due to flexibility in that region. Despite the weak linker density, the ligand could be unambiguously placed (because of the electron densities at the outer binding cavity) and was included in the crystallographic refinement. Due to the 2-fold crystallographic symmetry axis bisecting the binding channel, a statistical disorder model was applied, giving rise to two ligand binding modes per tetrameric TTR. After several cycles

of simulated annealing and subsequent positional and temperature factor refinement, water molecules were placed into the difference Fourier maps. The final cycle of map fitting was done using the unbiased weighted electron density map calculated by the shake/warp bias removal protocol.[69] Both of the symmetry related binding conformations of the ligand in each binding pocket were in good agreement with unbiased annealed omit maps as well as the shake/warp unbiased weighted maps phased in the absence of the inhibitor. The final cycle of refinement was carried out by the maximum likelihood method using CCP4-Refmac.[74,75] The nine *N*-terminal and three *C*-terminal residues were not included in the final model because of the lack of interpretable electron densities in the final map. A summary of the crystallographic analysis data is presented in Table S4.

Acknowledgment. We thank the National Institute of General Medical Sciences, the National Institutes of Health (GM 28384 and DK 46335), the W. M. Keck Foundation, the Skaggs Institute for Chemical Biology, the Lita Annenberg Hazen Foundation, and the Robert A. Welch Foundation (J.C.S.) for financial support. Use of BioCARS Sector 14 at the Advanced Photon Source was supported by the National Institutes of Health, National Centerfor Research Resources. The technical expertise of M. T. Dendle, R. Luke Wiseman, and Mike Saure is also greatly appreciated.

Supporting Information Available: Experimental data for the hydrazone library preparation and TTR fibril formation inhibition results, and synthesis and characterization details for oxime ethers **2/3/4a**−**l**, **1e**, **5d**−**f**, **7e**, and **8e**−**f** can be found, along with AUC traces for TTR·(**8f**)$_2$ under amyloidogenic conditions, fibril formation results for oxime ether and hydrazone degradation products, and TTR·(**5d**)$_2$ X-ray crystal structure data. This material is available free of charge via the Internet at http://pubs.acs.org.

References

(1) Sekijima, Y.; Hammarström, P.; Matsumura, M.; Shimizu, Y.; Iwata, M.; Tokuda, T.; Ikeda, S.; Kelly, J. W. Energetic Characteristics of the New Transthyretin Variant A25T May Explain Its Atypical Central Nervous System Pathology. *Lab. Invest.* **2003**, *83*, 409−417.

(2) Hammarström, P.; Sekijima, Y.; White, J. T.; Wiseman, R. L.; Lim, A.; Costello, C. E.; Altland, K.; Garzuly, F.; Budka, H.; Kelly, J. W. D18G Transthyretin Is Monomeric, Aggregation Prone, and Not Detectable in Plasma and Cerebrospinal Fluid: A Prescription for Central Nervous System Amyloidosis? *Biochemistry* **2003**, *42*, 6656−6663.

(3) Garzuly, F.; Wisniewski, T.; Brittig, F.; Budka, H. Familial meningocerebrovascular amyloidosis, Hungarian type, with mutant transthyretin (TTR Asp18Gly). *Neurology* **1996**, *47*, 1562−1567.

(4) Ikeda, S.; Nakazato, M.; Ando, Y.; Sobue, G. Familial *trans*-thyretin-type amyloid polyneuropathy in Japan: Clinical and genetic heterogeneity. *Neurology* **2002**, *58*, 1001−1007.

(5) Westermark, P.; Sletten, K.; Johansson, B.; Cornwell, G. G., III. Fibril in senile systemic amyloidosis is derived from normal transthyretin. *Proc. Natl. Acad. Sci. U.S.A.* **1990**, *87*, 2843−2845.

(6) Jacobson, D. R.; Pastore, R. D.; Yaghoubian, R.; Kane, I.; Gallo, G.; Buck, F. S.; Buxbaum, J. N. Variant-Sequence Transthyretin (Isoleucine 122) In Late-Onset Cardiac Amyloidosis In Black Americans. *N. Engl. J. Med.* **1997**, *336*, 466−473.

(7) Sipe, J. D. Amyloidosis. *Crit. Rev. Clin. Lab. Sci.* **1994**, *31*, 325−354.

(8) White, J. T.; Kelly, J. W. Support for the multigenic hypothesis of amyloidosis: The binding stoichiometry of retinol-binding protein, vitamin A, and thyroid hormone influences transthyretin amyloidogenicity in vitro. *Proc. Natl. Acad. Sci. U.S.A.* **2001**, *98*, 13019−13024.

(9) Hammarström, P.; Jiang, X.; Hurshman, A. R.; Powers, E. T.; Kelly, J. W. Sequence-dependent denaturation energetics: A major determinant in amyloid disease diversity. *Proc. Natl. Acad. Sci. U.S.A.* **2002**, *99*, 16427−16432.

(10) Herlenius, G.; Wilczek, H. E.; Larsson, M.; Ericzon, B.-O. Ten Years of International Experience With Liver Transplantation For Familial Amyloidotic Polyneuropathy: Results From the Familial Amyloidotic Polyneuropathy World Transplant Registry. *Transplantation* **2004**, *77*, 64−71.

(11) Olofsson, B.-O.; Backman, C.; Karp, K.; Suhr, O. B. Progression of cardiomyopathy after liver transplantation in patients with familial amyloidotic polyneuropathy, portuguese type. *Transplantation* **2002**, *73*, 745−751.

(12) Hammarström, P.; Wiseman, R. L.; Powers, E. T.; Kelly, J. W. Prevention of Transthyretin Amyloid Disease by Changing Protein Misfolding Energetics. *Science* **2003**, *299*, 713−716.

(13) Coelho, T.; Carvalho, M.; Saraiva, M. J.; Alves, I.; Almeida, M. R.; Costa, P. P. A strikingly benign evolution of FAP in an individual found to be a compound heterozygote for two TTR mutations: TTR Met 30 and TTR Met 119. *J. Rheumatol.* **1993**, *20*, 179.

(14) Coelho, T.; Chorão, R.; Sausa, A.; Alves, I.; Torres, M. F.; Saraiva, M. J. M. Compound heterozygotes of transthyretin Met30 and transthyretin Met119 are protected from the devastating effects of familial amyloid polyneuropathy. *Neuromusc. Disord.* **1996**, *6*, 27.

(15) Sacchettini, J. C.; Kelly, J. W. Therapeutic Strategies for Human Amyloid Diseases. *Nat. Rev. Drug Discuss.* **2002**, *1*, 267−275.

(16) Cohen, F. E.; Kelly, J. W. Therapeutic approaches to protein-misfolding diseases. *Nature* **2003**, 426, *6968*, 905−909.

(17) De Lorenzi, E.; Giorgetti, S.; Grossi, S.; Merlini, G.; Caccialanze, G.; Bellotti, V. Pharmaceutical Strategies Against Amyloidosis: Old and New Drugs in Targeting a "Protein Misfolding Disease." *Curr. Med. Chem.* **2004**, *11*, 1065−1084.

(18) Hardy, J.; Selkoe, D. J. The Amyloid Hypothesis of Alzheimer's Disease: Progress and Problems on the Road to Therapeutics. *Science* **2002**, *297*, 353−356.

(19) Ray, S. S.; Lansbury, P. T., Jr. A possible therapeutic target for Lou Gehrig's disease. *Proc. Natl. Acad. Sci. U.S.A.* **2004**, *101*, 5701−5702.

(20) Miller, S. R.; Sekijima, Y.; Kelly, J. W. Native state stabilization by NSAIDs inhibits transthyretin amyloidogenesis from the most common familial disease variants. *Lab. Invest.* **2004**, *84*, 545−552.

(21) Blake, C. C.; Geisow, M. J.; Swan, I. D. A.; Rerat, C.; Rerat, B. Structure of Human Plasma Prealbumin at 2.5 Å Resolution: A Preliminary Report on the Polypeptide Chain Conformation, Quaternary Structure and Thyroxine Binding. *J. Mol. Biol.* **1974**, *88*, 1−12.

(22) Blake, C. C.; Geisow, M. J.; Oatley, S. J.; Rerat, B.; Rerat, C. Structure of Prealbumin: Secondary, Tertiary and Quaternary Interactions Determined by Fourier Refinement at 1.8 Å. *J. Mol. Biol.* **1978**, *121*, 339−56.

(23) Bartalena, L.; Robbins, J. Thyroid Hormone Transport Proteins. *Clin. Lab. Med.* **1993**, *13*, 583−598.

(24) Schreiber, G.; Richardson, S. J. The Evolution of Gene Expression, Structure and Function of Transthyretin. *Comp. Biochem. Physiol. B Biochem. Mol. Biol.* **1997**, *116*, 137−160.

(25) Stockigt, J. R. Thyroid Hormone Binding and Metabolism. *Endocrinology, Fourth Ed.* Degroot, L. J., Jameson, J. L., Eds.; W. B. Saunders Co.: Philadelphia, 2001; Vol. 2, Chapter 94, pp 1314−1326.

(26) Colon, W.; Kelly, J. W. Partial Denaturation of Transthyretin Is Sufficient for Amyloid Fibril Formation in Vitro. *Biochemistry* **1992**, *31*, 8654−8660.

(27) Hammarström, P.; Schneider, F.; Kelly, J. W. *Trans*-Suppression of Misfolding in an Amyloid Disease. *Science* **2001**, *293*, 2459−2462.

(28) Lai, Z.; Colon, W.; Kelly, J. W. The Acid-Mediated Denaturation Pathway of Transthyretin Yields a Conformational Intermediate That Can Self-Assemble into Amyloid. *Biochemistry* **1996**, *35*, 6470−6482.

(29) Lashuel, H. A.; Lai, Z.; Kelly, J. W. Characterization of the Transthyretin Acid Denaturation Pathways by Analytical Ultracentrifugation: Implications for the Wild-Type, V30M, and L55P Amyloid Fibril Formation. *Biochemistry* **1998**, *37*, 17851−17864.

(30) Jiang, X.; Smith, C. S.; Petrassi, H. M.; Hammarström, P.; White, J. T.; Sacchettini, J. C.; Kelly, J. W. An Engineered Transthyretin Monomer that Is Nonamyloidogenic, Unless It Is Partially Denatured. *Biochemistry* **2001**, *40*, 11442−11452.

(31) Liu, K.; Cho, H. S.; Lashuel, H. A.; Kelly, J. W.; Wemmer, D. E. A glimpse of a possible amyloidogenic intermediate of transthyretin. *Nat. Struct. Biol.* **2000**, *7*, 754−757.

(32) Miroy, G. J.; Lai, Z.; Lashuel, H. A.; Peterson, S. A.; Strang, C.; Kelly, J. W. Inhibiting transthyretin amyloid fibril formation via protein stabilization. *Proc. Natl. Acad. Sci. U.S.A.* **1996**, *93*, 15051−15056.

(33) Peterson, S. A.; Klabunde, T.; Lashuel, H.; Purkey, H.; Sacchettini, J. C.; Kelly, J. W. Inhibiting transthyretin conformational changes that lead to amyloid fibril formation. *Proc. Natl. Acad. Sci. U.S.A.* **1998**, *95*, 12956−12960.

(34) Petrassi, H. M.; Johnson, S. M.; Purkey, H. E.; Chiang, K. P.; Walkup, T.; Jiang, X.; Powers, E. T.; Kelly, J. W. Potent and Selective Structure-Based Dibenzofuran Inhibitors of Transthyretin Amyloidogenesis: Kinetic Stabilization of the Native State. *J. Am. Chem. Soc.* In press.

(35) Purkey, H. E.; Palaninathan, S. K.; Kent, K. C.; Smith, C.; Safe, S. H.; Sacchettini, J. C.; Kelly, J. W. Hyrdoxylated Polychlorinated Biphenyls Selectively Bind Transthyretin in Blood and Inhibit Amyloidogenesis: Rationalizing Rodent PCB Toxicity. *Chem. Biol.* **2004**, *11*, 1719−1728.
(36) Adamski-Werner, S. L.; Palaninathan, S. K.; Sacchettini, J. C.; Kelly, J. W. Diflunisal Analogues Stabilize the Native State of Transthyretin. Potent Inhibition of Amyloidogenesis. *J. Med. Chem.* **2004**, *47*, 355−374.
(37) Green, N. S.; Palaninathan, S. K.; Sacchettini, J. C.; Kelly, J. W. Synthesis and Characterization of Potent Bivalent Amyloidosis Inhibitors That Bind Prior to Transthyretin Tetramerization. *J. Am. Chem. Soc.* **2003**, *125*, 13404−13414.
(38) Petrassi, H. M.; Klabunde, T.; Sacchettini, J.; Kelly, J. W. Structure-Based Design of *N*-Phenyl Phenoxazine Transthyretin Amyloid Fibril Inhibitors. *J. Am. Chem. Soc.* **2000**, *122*, 2178−2192.
(39) Baures, P. W.; Peterson, S. A.; Kelly, J. W. Discovering Transthyretin Amyloid Fibril Inhibitors by Limited Screening. *Bioorg. Med. Chem.* **1998**, *6*, 1389−1401.
(40) Oza, V. B.; Petrassi, H. M.; Purkey, H. E.; Kelly, J. W. Synthesis and Evaluation of Anthranilic Acid-Based Transthyretin Amyloid Fibril Inhibitors. *Bioorg. Med. Chem. Lett.* **1999**, *9*, 1−6.
(41) Baures, P. W.; Oza, V. B.; Peterson, S. A.; Kelly, J. W. Synthesis and Evaluation of Inhibitors of Transthyretin Amyloid Formation Based on the Nonsteroidal Antiinflammatory Drug, Flufenamic Acid. *Bioorg. Med. Chem.* **1999**, *7*, 1339−1347.
(42) Klabunde, T.; Petrassi, H. M.; Oza, V. B.; Raman, P.; Kelly, J. W.; Sacchettini, J. C. Rational design of potent human transthyretin amyloid disease inhibitors. *Nat. Struct. Biol.* **2000**, *7*, 312−321.
(43) Oza, V. B.; Smith, C.; Raman, P.; Koepf, E. K.; Lashuel, H. A.; Petrassi, H. M.; Chiang, K. P.; Powers, E. T.; Sacchettini, J.; Kelly, J. W. Synthesis, Structure, and Activity of Diclofenac Analogues as Transthyretin Amyloid Fibril Formation Inhibitors. *J. Med. Chem.* **2002**, *45*, 321−332.
(44) Razavi, H.; Palaninathan, S. K.; Powers, E. T.; Wiseman, R. L.; Purkey, H. E.; Mohamedmohaideen, N. N.; Deechonkit, S.; Chiang, K. P.; Dendle, M. T. A.; Sacchettini, J. C.; Kelly, J. W. Benzoxazoles as Transthyretin Amyloid Fibril Inhibitors: Synthesis, Evaluation, and Mechanism of Action. *Angew. Chem., Int. Ed.* **2003**, *42*, 2758−2761.
(45) Nazarpack-Kandlousy, N.; Zweigenbaum, J.; Henion, J.; Eliseev, A. V. Synthesis and Characterization of a Mixture-Based Library of Oxime Ethers Based on a Common Aromatic Scaffold. *J. Comb. Chem.* **1999**, 199−206.
(46) Hochgürtel, M.; Kroth, H.; Piecha, D.; Hofmann, M. W.; Nicolau, C.; Krause, S.; Schaaf, O.; Sonnenmoser, G.; Eliseev, A. V. Target-induced formation of neuraminidase inhibitors from in vitro virtual combinatorial libraries. *Proc. Nat. Acad. Sci., U.S.A.* **2002**, *99*, 3382−3387.
(47) FDA approved antibacterial agents containing the oxime ether moiety were found using MDL ISIS/Base 2.5, from MDL Information Systems, Inc., and MDDR 2003.2 (25.11) database, which scans the Drug Data Report from Prous Science Publishers containing data regarding the development of pharmaceuticals.
(48) Purkey, H. E.; Dorrell, M. I.; Kelly, J. W. Evaluating the binding selectivity of transthyretin amyloid fibril inhibitors in blood plasma. *Proc. Natl. Acad. Sci. U.S.A* **2001**, *98*, 5566−5571.
(49) Karabatsos, G. J.; Graham, J. D.; Vane, F. M. *syn-anti* Isomer Determination of 2,4-Dinitrophenylhydrazones and Semicarbazones by N.m.r. *J. Am. Chem. Soc.* **1962**, *84*, 753−755.
(50) Lustig, E. A Nuclear Magnetic Resonance Study of *syn-anti* Isomerism in Ketoximes. *J. Phys. Chem.* **1961**, *65*, 491−495.
(51) Karabatsos, G. J.; Shapiro, B. L.; Vane, F. M.; Fleming, J. S.; Ratka, J. S. Structural Studies by Nuclear Magnetic Resonance. II. Aldehyde 2,4-Dinitrophenylhydrazones. *J. Am. Chem. Soc.* **1963**, *85*, 2784−2788.
(52) Karabatsos, G. J.; Taller, R. A. Structural Studies by Nuclear Magnetic Resonance. V. Phenylhydrazones. *J. Am. Chem. Soc.* **1963**, *85*, 3624−3629.
(53) Sheradsky, T.; Nov, E. Studies on the Preparation of *N*-Alkyl-*O*-phenylhydroxylamines. *J. Chem. Soc., Perkin Trans. 1* **1980**, *12*, 2781−2786.
(54) Karabatsos, G. J.; His, N. Structural Studies by Nuclear Magnetic Resonance −XI. Conformations and Configurations of Oxime *O*-Methyl Ethers. *Tetrahedron* **1967**, *23*, 1079−1095.
(55) Rappoport, Z.; Sheradsky, T. The Ultraviolet Spectra of *O*-(2,4-Dinitrophenyl)oximes and 2,4-Dinitrophenylhydrazones: Transmission of Electronic Effects through O and NH groups. *J. Chem. Soc. B, Phys. Org.* **1967**, *9*, 898−903.
(56) Abele, E.; Lukevics, E. Recent Advances in the Chemistry of Oximes. *Org. Prep. Proced. Int.* **2000**, *32*, 235−264.
(57) Petrassi, H. M.; Sharpless, K. B.; Kelly, J. W. The Copper-Mediated Cross-Coupling of Phenylboronic Acids and *N*-Hydroxyphthalimide at Room Temperature: Synthesis of Aryloxyamines. *Org. Lett.* **2001**, *3*, 139−142.
(58) Miyazawa, E.; Sakamoto, T.; Kikugawa, Y. Preparation of Ring-Substituted Phenoxyamine Derivatives. *Org. Prep. Proced. Int.* **1997**, *29*, 594−600.
(59) Choong, I. C.; Ellman, J. A. Synthesis of Alkoxylamines by Alkoxide Amination with 3,3′-Di-*tert*-butyloxaziridine. *J. Org. Chem.* **1999**, *64*, 6528−6529.
(60) Miller, M. J.; Loudon, G. M. A Convenient, High-Yield Conversion of Aldehydes to Nitriles. *J. Org. Chem.* **1975**, *40*, 126−127.
(61) Supsana, P.; Tsouongas, P. G.; Varvounis, G. A novel one-pot synthesis of isomeric naphtha[1,2-*d*]isoxazole-2-oxide and naphtha[1,8-*de*][1,2]oxazine ring systems. A case of simultaneous *o*- and *peri*-cyclisation in naphthalene. *Tetrahedron Lett.* **2000**, *41*, 1845−1847.
(62) Knudsen, R. D.; Snyder, H. R. A Convenient One-Step Conversion of Aromatic Nitro Compounds to Phenols. *J. Org. Chem.* **1974**, *39*, 3343−3346.
(63) Gómez, V.; Pérez-Medrano, A. Synthesis of β-Dicarbonyl Compounds via the Conjugate Addition of Benzaldoximate Anion to α,β-Acetylenic Carbonyl Compounds. *J. Org. Chem.* **1994**, *59*, 1219−1221.
(64) Cho, B. R.; Min, B. M.; Lee, C. W.; Je, J. T. Reactions of (*E*)-*O*-Arylbenzaldoximes with Secondary Amines in Acetonitrile. Competition between E2 and S_NAr Reactions. *J. Org. Chem.* **1991**, *56*, 5513−5517.
(65) Royer, R. E.; Deck, L. M.; Campos, N. M.; Hunsaker, L. A.; Vander Jagt, D. L. Biologically Active Derivatives of Gossypol: Synthesis and Antimalarial Activities of Peri-Acylated Gossylic Nitriles. *J. Med. Chem.* **1986**, *29*, 1799−1801.
(66) Castellino, A. J.; Rapoport, H. Syntheses of Tetrahydrofuro[2,3-*b*]benzofurans: A Synthesis of (±)-Aflatoxin B_2. *J. Org. Chem.* **1986**, *51*, 1006−1011.
(67) Blake, J. A.; Pratt, D. A.; Lin, S.; Walton, J. C.; Mulder, P.; Ingold, K. U. Thermolyses of *O*-Phenyl Oxime Ethers. A New Source of Iminyl Radicals and a New Source of Aryloxyl Radicals. *J. Org. Chem.* **2004**, *69*, 3112−3120.
(68) Petitpas, I.; Petersen, C. E.; Ha, C. E.; Bhattacharya, A. A.; Zunszain, P. A.; Ghuman, J.; Bhagavan, N. V.; Curry, S. Structural Basis of Albumin-Thyroxine Interactions and Familial Dysalbuminemic Hyperthyroxinemia. *Proc. Nat. Acad. Sci., U.S.A.* **2003**, *100*, 6440−6445.
(69) Reddy, V.; Swanson, S. M.; Segelke, B.; Kantardjieff, K. A.; Sacchettini, J. C.; Rupp, B.Effective electron-density map improvement and structure validation on a Linux multi-CPU web cluster: The TB Structural Genomics Consortium Bias Removal Web Service. *Acta Crystallogr., Sect. D, Biol. Crystallogr.* **2003**, *59*, 2200−2210.
(70) Lashuel, H. A.; Wurth, C.; Woo, L.; Kelly, J. W. The Most Pathogenic Transthyretin Variant, L55P, Forms Amyloid Fibrils under Acidic Conditions and Protofilaments under Physiological Conditions. *Biochemistry* **1999**, *38*, 13560−13573.
(71) Schuster, T. M.; Laue, T. M.; Editors *Modern Analytical Ultracentrifugation: Acquisition and Interpretation of Data for Biological and Synthetic Polymer Systems*; Birkhauser: Boston, 1994.
(72) Otwinowski, Z.; Minor, W. Macromolecular Crystallography, Part A. In *Methods in Enzymology, 276: Macromolecular Crystallography, Part A*; Carter, C. W., Jr., Sweet, R. M., Eds.; Academic Press: New York, 1997, pp 307−326.
(73) Brunger, A. T.; Adams, P. D.; Clore, G. M.; DeLano, W. L.; Gros, P.; Grosse-Kunstleve, R. W.; Jiang, J.-S.; Kuszewski, J.; Nilges, N.; Pannu, N. S.; Read, R. J.; Rice, L. M.; Simonson, T.; Warren, G. L. Crystallography & NMR System: A New Software Suite for Macromolecular Structure Determination. *Acta Crystallogr., Sect. D, Biol. Crystallogr.* **1998**, *54*, 905−921.
(74) Bailey, S. The CCP4 Suite: Programs for Protein Crystallography. *Acta Crystallogr., Sect. D, Biol. Crystallogr.* **1994**, *50*, 760−763.
(75) Murshudov, G. N.; Vagin, A. A.; Dodson, E. J. Refinement of Macromolecular Structures by the Maximum-Likelihood Methodology. *Acta Crystallogr., Sect. D, Biol. Crystallogr.* **1997**, *53*, 240−255.

JM049274D